IEEE Access
Multidisciplinary | Rapid Review | Open Access Journal

Received May 1, 2020, accepted May 12, 2020, date of publication May 19, 2020, date of current version July 20, 2020.

Digital Object Identifier 10.1109/ACCESS.2020.2995581

Nonlinear Error Compensation of Capacitive Angular Encoders Based on Improved Particle Swarm Optimization Support Vector Machines

BO HOU[1], (Graduate Student Member, IEEE), BIN ZHOU[1], XIANG LI[1], LUYING YI[2], QI WEI[1], AND RONG ZHANG[1]

[1]Research Center for Navigation Technology, Department of Precision Instrument, Tsinghua University, Beijing 100084, China
[2]State Key Laboratory of Precision Measurement Technology and Instruments, Department of Precision Instrument, Tsinghua University, Beijing 100084, China

Corresponding authors: Bin Zhou (zhoub@mail.tsinghua.edu.cn), Qi Wei (weiqi@tsinghua.edu.cn), and Rong Zhang (rongzh@mail.tsinghua.edu.cn)

ABSTRACT Rotary encoders are widely applied in a variety of industrial fields. However, as the exist of the installation, processing and demodulation circuits errors, the test result of the encoder is superimposed with periodic nonlinear errors and the encoder needs compensation to achieve high measurement accuracy. Traditional methods including the least square method (LSM) and back propagation artificial neural network (BP-ANN), are not capable of addressing nonlinear errors. Thus, a novel method based on improved particle swarm optimization (IPSO) and support vector machines (SVM) is proposed to provide better compensation. The proposed method incorporates the SVM method into the design of the compensation model, and the IPSO algorithm is applied to tune the SVM parameters. To validate the algorithm, four sets of data were obtained from encoders with different numbers of segments. The experimental results show that the IPSO-SVM algorithm has a better prediction precision and the nonlinear standard deviation of 180 petal-shaped numbers has dropped from 0.08° to 0.0005° after compensation over 0° to 360° measurement range. Based on the results, the proposed IPSO-SVM model provided more accurate compensation on the nonlinear errors to the capacitive angular encoders than other method.

INDEX TERMS Capacitive encoder, nonlinear compensation, support vector machine, improved particle swarm optimization.

I. INTRODUCTION

Rotary encoders applied to measure the angular position and speed have been broadly utilized in industrial automation control systems [1]–[4]. They are expected to achieve high precision, high resolution and high reliability in harsh environments [5]–[7]. There are many types of encoders, such as, electromagnetic, inductive, capacitive, optical types. In recent years, the capacitive encoder which meets the requirement of small size, low power consumption and strong environmental adaptability has become the research hotspot. In capacitive encoder research filed, the single-excitation capacitance sensing encoder is the most prominent research [8]–[10]. The measurement principle of single-excitation capacitive encoder is similar to the inductive synchronizer and the capacitive encoder has good repeatability and high resolution.

However, as the influence of installation error, processing error and demodulation circuit error, a periodic nonlinear error exits in the measurement result. The researchers in [10] investigated the sources of these periodic nonlinear errors and introduced hardware methods to compensate for them. However, hardware based compensation is typically complicated and expensive [11] and is unable to fully eliminate the effects of periodic nonlinear errors. An alternative approach to improve the measurement precision is compensate the periodic nonlinear error by way of a software algorithm. Traditional software compensation approaches include the least squares method (LSM) and artificial neural network (ANN) [12]–[18]. While the LSM is commonly applied to error compensation, its accuracy is limited as it often

The associate editor coordinating the review of this manuscript and approving it for publication was Yongquan Sun.

identifies a local optimum rather than the global optimum when fitting periodic errors [16], [19]. With regard to ANN, studies have found that an ANN can overcome periodic nonlinear shortages and achieve a good fit [13], however, their disadvantages are a slow convergence rate, a tendency to over-fit, and a susceptibility to falling into a local extremum.

Compared to the LSM and ANN, the support vector machine (SVM) is a new regression method and owns good generalization ability [20]–[30]. Besides, SVM can be used to solve problems with only a few samples, accommodate nonlinear data, avoid local minima, and so on. However, the generalization ability and working performance of SVM relies on the selection of appropriate parameter. Choosing the appropriate learning parameters is very important for the learning performance and generalization ability of the SVM model, which directly affects the prediction accuracy. Traditional prediction methods often select parameters by trial and error according to experience, but this does not ensure that the training error of the SVM model reaches the global minimum, and the prediction results cannot guarantee to be the optimal results.

In this paper, the learning parameters of the SVM algorithm are optimized using the improved particle swarm optimization (PSO) method, which is a global parallel optimization method based on population that has the advantages of fast convergence and easy implementation. However, to overcome the shortcomings of the traditional PSO algorithm, such as slow convergence and the likelihood of falling into a local minimum, its performance was improved by reducing the speed and search range. These modifications were similar to those described for the restricted range PSO algorithm in [22], [23], [28], [31], [32]. In the following, the improved PSO algorithm is referred to as the IPSO algorithm and is used for the optimal selection of SVM learning parameters. As will be shown, the results of the analysis confirm the effectiveness of the IPSO algorithm in optimizing the selection of SVM learning parameters to provide more accurate and stable parametric predictions in nonlinear method.

The paper is organized as follows. The measurement principles and nonlinear error compensation model are described in Section 2. The results of compensation via the LSM and artificial neural network (ANN) are presented in Section 3. The proposed IPSO tuning support vector machine (IPSO-SVM) is introduced in Sections 4 and 5, followed by a discussion of the results in Section 6. Finally, the conclusion is presented in Section 7.

II. ENCODER PRINCIPLE AND ERROR MODEL

A. MEASUREMENT PRINCIPLE

The capacitive angular encoder is fabricated by printed circuit board (PCB) technology and the principle is similar to inductive synchronizer. First, an excitation signal acted on the stator. Then, four feedback signals are available on the four sets of collection electrodes. More details about the measurement principle is presented in Ref. [8] and [10]. After differential amplification, the four voltage signals are converted into two

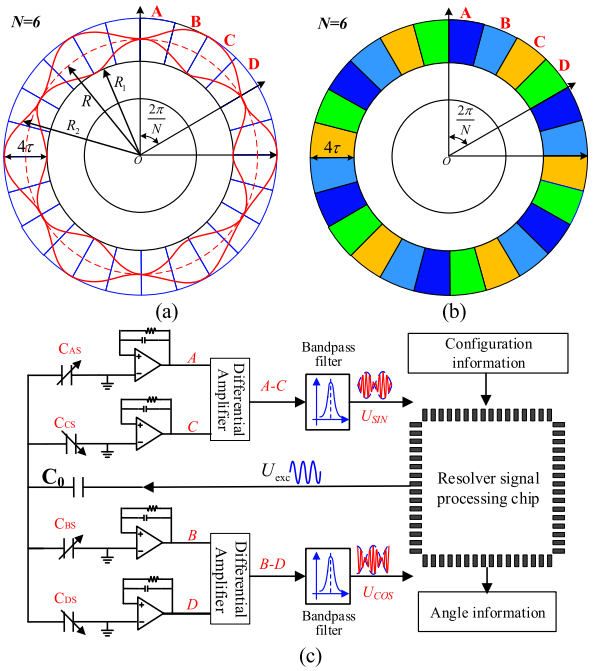

FIGURE 1. (a) model of the encoder, the division number N is equal to 6; (b) model of stator with four sets of colored collection electrodes; (c) schematic of demodulation circuit. More details are shown in Ref [8] and [10].

orthogonal amplitude modulated signals:

$$\begin{aligned} U_{SIN} &= U \cdot \sin(N\phi) \cdot \sin(wt) \\ U_{COS} &= U \cdot \cos(N\phi) \cdot \sin(wt), \end{aligned} \tag{1}$$

where $U \cdot \sin(wt)$ is the excitation signal, ϕ is the relative angle between the rotor and stator, and N is the division number which divides the mechanical angle from 0 toa 360° into an electrical angle of 0 to 360°/N to achieve high precision measurement. Then, the angle information can obtained after arctangent calculation via a resolver chip.

$$\theta = arc\tan(\frac{\sin(N \cdot \phi)}{\cos(N \cdot \phi)}) \tag{2}$$

The model of the capacitive encoder is presented in Figure 1(a) and the circuit schematic is shown in Figure 1(b).

B. NONLINEAR ERROR

Due to the installation, processing and demodulation circuit's errors, a period nonlinear errors is superimposed in the final measurement result as shown in Figure 2(a). The spectral analysis of nonlinear errors is shown in Figure 2(b), and it is obvious that the result includes DC error, mechanical period error, and electrical period error [6], [12].

The periodic nonlinear error in the test results greatly limits the measurement accuracy of the encoder. Further, the repeatability of the encoder was tested. The test results showed that the repeated error did not exceed 0.0005°. Excellent repeatability indicates that the capacitive angular encoder can achieve high measurement accuracy through compensation. The compensation model is shown in the Figure 3. Therefore, the quality of the compensation algorithm becomes the key to improve the accuracy of the sensor.

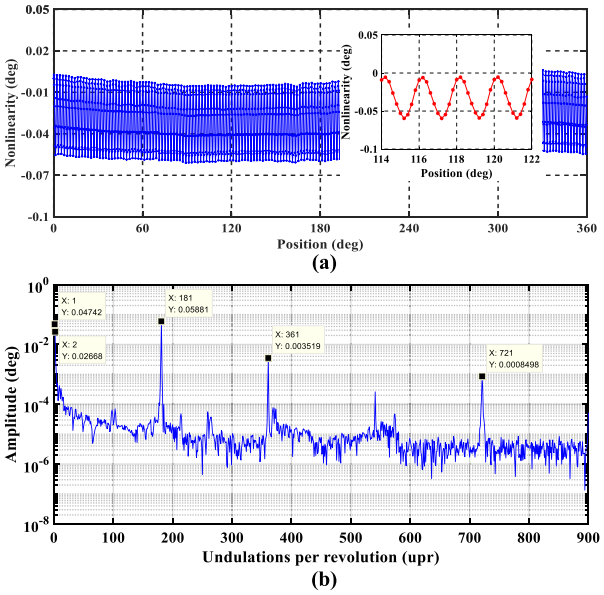

FIGURE 2. (a) Nonlinearity over a full measurement range of an encoder with subdivide number of 180. And the nonlinearity error has been obtained by compare the encoder output with the turntable output. (b) Spectral analysis of the nonlinear errors, which include DC, mechanical, and electrical cycle errors (corresponding to 0 upr, 1 upr, 180 upr, 360 upr and 720 upr).

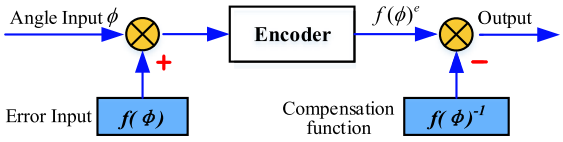

FIGURE 3. The schematic diagram of compensation model.

An accurate error fitting model can greatly improve the compensation accuracy of the sensor.

The actual angular output transfer function is expressed,

$$f(\phi)^e = \phi + f(\phi) \tag{3}$$

To achieve high-precision measurement, the most appealing method is to construct an accurate compensation model function $f(\phi)^{-1}$.

III. COMPENSATION VIA LSM AND BP-ANN

If the compensation function $f(\phi)^{-1}$ is exactly the inverse of the transfer function of the encoder, the compensation result will remain consistent with the input angle and the errors caused by the installation, processing, and demodulation circuits will be eliminated. After analyzing the nonlinear error via the fast Fourier transform, it was found that the error curve of the capacitive angle encoder is periodic. Thus, the compensation function can be constructed in the form of a multi-order sine function:

$$\begin{aligned} f(\phi)^{-1} = {} & d + A_0 \sin(\phi + \beta_0) + A_1 \sin(N \cdot \phi + \beta_1) \\ & + A_2 \sin(2N \cdot \phi + \beta_2) + A_3 \sin(3N \cdot \phi + \beta_3) \\ & + A_4 \sin(4N \cdot \phi + \beta_4) \end{aligned} \tag{4}$$

The parameters of the function can be obtained via the LSM method. The encoder with 180 segments after compensation via the LSM are shown in Figure 4.

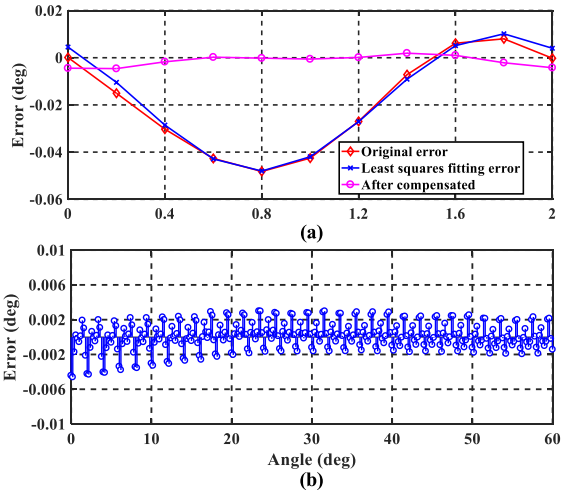

FIGURE 4. Nonlinear errors after compensation via the LSM. (a) The original error, least squares fitting function, and compensated error within one electronic period (0-2°). (b) The compensation error over the range from 0 to 60°.

Compare Figure 4(b) with Figure 2(a), it can be seen that the maximum nonlinear error decreased from 0.08° to 0.006° over all the measurement range. However, the residual error still remains large and exhibits obvious periodic characteristics. As the formula used for LSM fitting cannot fully represent the characteristics of nonlinear errors, the compensation provided by the LSM was inadequate. To address this, another nonlinear algorithm will be selected for compensation purposes.

Besides the LSM, the ANN algorithm has been conducted to compensate the nonlinear error. The artificial neural network methods has been widely used in many applications. The experiment is conducted via the Neural Net Fitting toolbox in MATLAB. In experiment, the training, validation, and testing percentages were 70%, 15%, and 15%, and the number of hidden neurons was 20. The results of compensation via the BP-ANN are shown in Figure 5.

It can be seen that the error in the electrical cycle can be effectively suppressed and the BP-ANN fitting error is more consistent with the original error. The nonlinear error of the capacitive encoder compensated by the BP-ANN has been obviously reduced from 0.08° to 0.005° over all the measurement range. Compare Figure 5(a) with Figure 4(a), the conclusion can be obtained that BP-ANN shows a better compensation than LSM in electrical cycle (0° - 2°). However, the compensated error is slowly changing over the entire measurement range as shown in Figure 5(b). With the ANN algorithm it is difficult to achieve an effective compensation for periodic nonlinear errors over a full scale range of 0° to 360°. In order to achieve higher measurement precision, the nonlinear error is compensated by IPSO-SVM.

IV. SUPPORT VECTOR MACHINE (SVM) ALGORITHM

SVM is a machine learning algorithm, which is proposed in 1995 by Vapnik and Cortes. The main concept of support vector machine is to try to transform the data on input space to a high dimensional feature space via a nonlinear

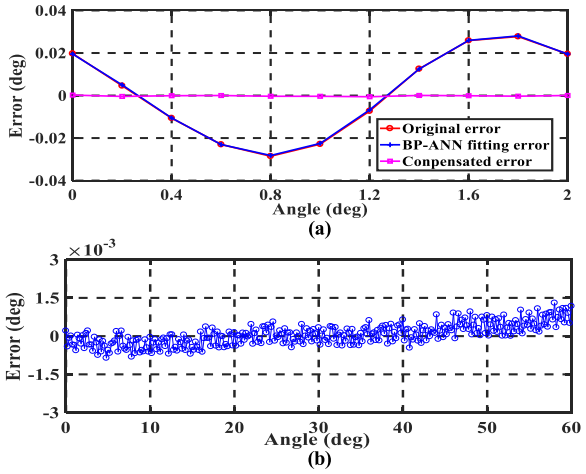

FIGURE 5. Sensor measurement errors after compensation by the ANN. (a) Original error, least squares fitting function, and compensation error within one electronic period (0-2°). Note that the BP-ANN fitting error is very consistent with the original error. (b) The compensation error from 0° to 60°. Note that the error changes slowly over the measurement range.

mapping, then conduct the linear regression operations in the high dimensional feature space. Compared LSM and ANN, SVM effectively improves the calculation accuracy and convergence speed.

SVM can be described as follows. Assume (x_i, y_i) are training data sets, where x_i is the input data and y_i is the corresponding nonlinear error value. The basic idea of SVM is try to map the input data x_i to a high dimensional feature space by way of a nonlinear mapping $\varphi(x_i)$, then try to conduct linear regression operations in this space. The function can be expressed as follows:

$$\min\ J(\omega, \xi) = \frac{1}{2}\omega^T\omega + \frac{C}{2}\sum_{i=1}^{l}\xi_i^2 \tag{5}$$

$$s.t.\ y_i = \omega^T\varphi(x_i) + b + \omega + \varsigma_i \quad (i = 1, 2, \ldots, l) \tag{6}$$

where $x_i \in R^l$ and $y_i \in R$ represent the input and output vectors of the model, J is defined as a loss function, w is a weight vector, T denotes a vector transposition, $\varsigma_i \in R$ is an empirical error, b is an offset, $C \in R^+$ is a penalty parameter, and $\varphi(x_i)$ is a nonlinear mapping from the input space to the feature space. To solve the mentioned constrained optimization problem, the Lagrange polynomial function of the dual problem can be presented as:

$$L(\omega, b, \xi, \alpha) = J(\omega, \xi) - \sum_{i=1}^{l}\alpha_i(\omega^T\varphi(x_i) + b + \xi_i - y_i) \tag{7}$$

where α_i represents a Lagrange multiplier, and, by the Karush–Kuhn–Tucker condition, $\omega\, b\, \xi\, \alpha$ can be solved by partial derivatives and set equal to zero. The following linear equation can be obtained by eliminating ω, ξ_i.

$$\begin{bmatrix} 0 & I^T \\ I & \Omega + C^{-1}E \end{bmatrix} \times \begin{bmatrix} b \\ a \end{bmatrix} = \begin{bmatrix} 0 \\ y \end{bmatrix} \tag{8}$$

where $I = [1, 1, \cdots, 1]^T$, E is identity matrix; $a = [a_1, a_2, \cdots, a_l]^T y = [y_1, y_2, \cdots, y_l]^T$, and $\Omega_{ij} = \varphi(x_i) \cdot \varphi(x_j) = K(x_i, x_j)$ are kernel functions that satisfy Mercer's condition. Note that there are many types of kernel functions that can be used as least squares support vector regression (LSSVR) kernel functions and satisfy this condition. While there are differences between various kernel functions, there is no unified standard describing kernel selection in SVM applications. In this paper, the Gaussian RBF kernel function with a limited number of parameters and a strong learning ability was selected for use in the LSSVM model. The LSSVM decision function obtained by solving the above equation is:

$$f(x) = \sum_{i=1}^{l} a_i \times \exp(-\frac{\|x_i - x_j\|^2}{2\sigma^2}) + b \tag{9}$$

where x_i represents any input sample vector, x_j represents the center of the Gaussian RBF kernel function, and σ represents the width of the Gaussian RBF kernel function.

The generalization and learning abilities of the SVM are determined by parameters. The penalty parameter C and the width of RBF kernel function σ are directly related to the prediction efficiency and accuracy of the model. The penalty parameter C affects generalization and empirical error. Larger values of C will increase the complexity of the model and make it more susceptive to overfitting, and, smaller values of C will reduce the complexity of the model, making it more susceptible to over fitting. In next study, the improved PSO algorithm was used to optimize parameters C and σ to achieve better prediction results.

V. PARAMETERS OPTIMIZATION BY IMPROVED PSO ALGORITHM

The particle swarm optimization (PSO) algorithm is a random search algorithm based on group collaboration developed by simulating bird foraging behavior. First, a group of random particles (random solutions) is initialized, all of which have an associated fitness value from the optimized function and a speed to determine its flight direction and distance. In operation, particles in a swarm follow the current best particle while searching the solution space until the best solution is finally identified. Updating the particle position in each iteration is accomplished by tracking two extrema. The first is the best solution found by the particle itself, i.e., the individual extremum, and second is the best solution identified by the entire population of the swarm, i.e., the global extremum.

The equations used to update each particle's position and velocity are shown as follows:

$$V_{id}^{k+1} = \omega V_{id}^k + c_1 r_1 (p_{\mathrm{id}}^k - x_{id}^k) + c_2 r_2 (p_{gd}^k - x_{id}^k) \tag{10}$$

$$X_{id}^{k+1} = X_{id}^k + V_{id}^{k+1} \tag{11}$$

where ω is the inertia factor; c_1 and c_2 are the learning or acceleration factors, and are usually equal to 2; r_1 and r_2 are random numbers distributed in the interval [0,1]; $V_{\max}$ represents the maximum speed that can be achieved by a particle; p_i^k represents the d-th dimension of the individual extremum of the I-th variable; and p_{gd}^k represents the d-th dimension of the global optimal solution.

In an implementation of the PSO algorithm, parameters ω, c_1, c_2, r_1, and r_2 all significantly affect the convergence of the algorithm. The common PSO algorithm has a fast convergence speed, but, it converges slower in the later stages. To improve the solution quality and speed up the convergence speed, the following three strategies were applied to improve the PSO algorithm:

- **Particle Velocity**

At the completion of each fitness calculation, the current speed is compared to the initial speed before updating the position to ensure the speed is within the initially specified range. The initial range of the random particle position is defined as:

$$(\mathrm{x}_j^{\min} - \varepsilon) - x_{ij}^0 \le x_{ij}^0 \le (\mathrm{x}_j^{\max} + \varepsilon) - x_{ij}^0, \tag{12}$$

where ε is a tiny positive real number, $\mathrm{x}_j^{\min}$ and $\mathrm{x}_j^{\max}$ are the minimum and maximum positions of the particle, respectively, and x_{ij}^0 is the original position of the particle. The initial velocity of the particle is randomly selected within a certain range. At (k + 1) iterations, the velocity limit of element j of particle i is:

$$\mathrm{V}_{ij}^{k+1} = \begin{cases} \mathrm{V}_{ij}^{\max}, & \mathrm{V}_{ij}^{k+1} \ge \mathrm{V}_{ij}^{\max} \\ \mathrm{V}_{ij}^{k+1}, & -\mathrm{V}_{ij}^{\max} \ge \mathrm{V}_{ij}^{k+1} \ge -\mathrm{V}_{ij}^{\max} \\ \text{-}\mathrm{V}_{ij}^{\max}, & \mathrm{V}_{ij}^{k+1} \ge -\mathrm{V}_{ij}^{\max}, \end{cases} \tag{13}$$

where $V_{ij}^{\max} = (X_j^{\max} - X_j^{\min}) \Big/ R$ and R is a real number in the range [5], [10]; V_{ij}^{k+1} is the velocity at which the particle iterates (k + 1) times; and $V_{ij}^{\max}$ is the maximum velocity of the particle.

- **Particle Search Space**

Reducing the search space is conducive to speeding up the convergence. In this case, the search space is dynamically adjusted to reach the expected range. First, the minimum and maximum values of control variable j in particle i are limited:

$$\begin{aligned} X_{j,\max}^0 &= X_j^{\max}, \\ X_{j,\min}^0 &= X_j^{\min}. \end{aligned} \tag{14}$$

After $(k + 1)$ iterations, the search space is limited to:

$$\begin{aligned} X_{j,\max}^{k+1} &= X_{j,\max}^k - (X_{j,\max}^k - gbest_j^k)\Delta, \\ X_{j,\min}^{k+1} &= X_{j,\min}^k - (gbest_j^k - X_{j,\min}^k)\Delta, \end{aligned} \tag{15}$$

where the optional range of Δ is (0, 1); $X_{j,\max}^{k+1}$ is the maximum position after $(k + 1)$ iterations; $X_{j,\max}^k$ is the maximum position after k iterations; $gbest_j^k$ is the global extremum of the particle after k iterations; $X_{j,\min}^{k+1}$ is the minimum position of the particle after $(k+1)$ iterations; and $X_{j,\min}^k$ is the position of the particle after the k-th iteration.

- **Crossover Operation**

A crossover operation was implemented as per the following equation:

$$\begin{aligned} cx_1 &= x_1 \cdot e + x_2 \cdot (1 - e) \\ cx_2 &= x_1 \cdot (1 - e) + x_2 \cdot e, \end{aligned} \tag{16}$$

where cx_1 and cx_2 are new particles generated by the crossover operation, x_1 and x_2 are parent particles, and e represents a D-dimensional random sequence of (0, 1) intervals.

After the crossover operation, the fitness value of the new particle is calculated, and if the fitness value improved, the original particle is replaced by the new particle. On the other hand, if the fitness value did not change, then a mutation operation is conducted to strengthen the search around the particle. After mutation, the particle with a higher fitness value is selected to replace the original particle. The mutation operation is defined as:

$$\begin{aligned} mx_1 &= x + (1 - \frac{t}{T})^a (ub - x) \\ mx_2 &= x - (1 - \frac{t}{T})^a (x - lb), \end{aligned} \tag{17}$$

where mx_1 and mx_2 are mutated particles and a is the weight of the variation.

Once the local search for the global best particle has been strengthened, a search is conducted around the optimal particle to improve the accuracy of the solution. The initial value of the SVM algorithm parameters can then be obtained based on the shrinkage of the adaptive PSO algorithm. The SVM algorithm is then applied to complete the error prediction model.

The process of applying the IPSO algorithm to optimize the parameters C and σ of SVM is depicted in Figure 6. The steps in the process are as follows.

Step 1 Initialize the number of IPSO algorithm parameters and the maximum number of iterations, set parameters such as particle velocity, weight, learning factor, and randomly initialize SVM parameters C and $\boldsymbol{\sigma}$.

Step 2: By evaluating the objective function of each particle, steady-state penalty function and transient stability simulation, the penalty function of transient stability of each particle is evaluated, and the current parameter value of the particle is evaluated.

Step 3: Calculate the fitness of each particle. The fitness value of each particle as the following equation:

$$f(C,\ g) = \sum_{i=1}^{n} (y_i - y_i')^2 / n, \tag{18}$$

where y_i is the nonlinear error value, y_i' is the fitted value and n is the number of input data.

Step 4: Update the velocity and position of each particle and evaluate the fitness value. Then, randomly select a new position in the neighborhood of the particle and compute the fitness value of the new position.

Step 5: Calculate the fitness values under different particles, consider the particle velocity and position when performing different particle calculations, and carry out the cross-variation operation.

Step 6: Determine if the current iteration is the last based on the limit. If so, then stop iterating and output the most suitable SVM parameter. Otherwise, recalculate the weight, position, and speed of the particle and return to Step 2

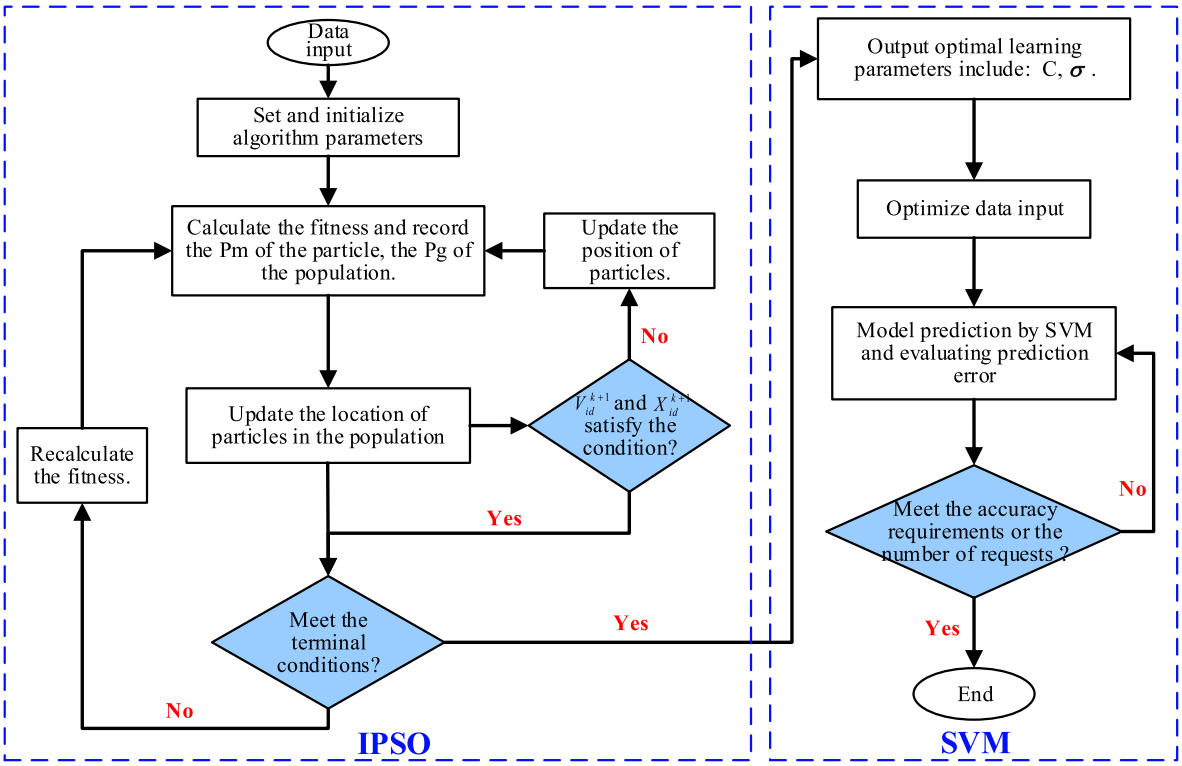

FIGURE 6. Flow chart of the proposed compensation method.

Step 7: Determine if the current iteration number is up to the maximum iterations or g_{best} is the lowest fitness value, then output the parameters C and σ. Otherwise, return to Step 2.

Step 8: Obtain the optimized SVM parameter, apply it to SVM to carry out error classification regression, and determine the high precision error compensation model.

VI. ENCODER COMPENSATION VIA THE IPSO-SVM

In this section, the performance of the proposed IPSO-SVM method was analyzed by applying it to a capacitive encoder. To ensure the algorithm was sufficiently versatile, experiments were conducted with several different subdivide numbers. A porotype with four channels (each channel's divide number is 119, 120, 179 and 180) is fabricated. The prototype is illustrated in Figure 7 and the experimental setup is presented in Figure 8. The setup included a high-precision turntable and the positional accuracy of the turntable is better than ±0.8 arcsec, and an encoder containing rotor, stator, and demodulation circuit.

Table 1 shows the initial values for the IPSO algorithm. Consider convergence time and compensation accuracy, the particles number and population size are set 50 and 20respectively. The evolutions number is set 20.

The optimal parameters (C and σ) after training by the IPSO model are listed in Table 2. Obtain the optimized SVM parameter, apply it to SVM to carry out error classification regression, and determine the high precision error compensation model.

The experiment is conducted, and the fitting curve and nonlinear error compensated by IPSO-SVM algorithm is shown in Figure 9, where it can be seen that the curve is consistent with the trends in the experimental samples. In essence, the IPSO-SVM model effectively compensated for the nonlinear error arising from the installation, processing, and demodulation circuits. The measurement error after compensated was less than 0.0005° over full measurement range. Additional experiments were conducted for different subdivide number, and the results are shown in Figure 10 to 12. It can be seen from these figures that the proposed method successfully compensated for the nonlinear errors in the capacitive angular encoder.

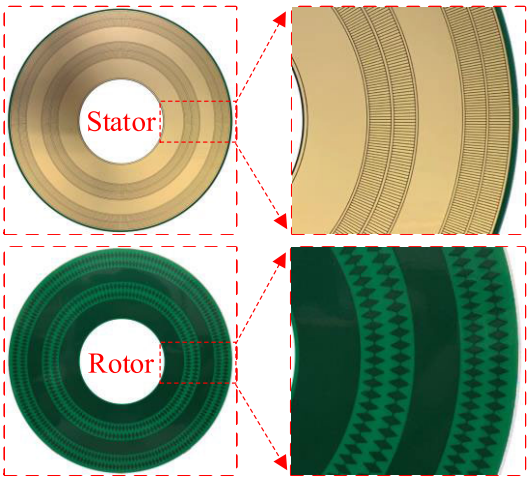

FIGURE 7. Sensitive structures of prototype including stator and rotor. The fabricated prototype with four channels and each channel's divide number is 180, 179, 120, and 119.

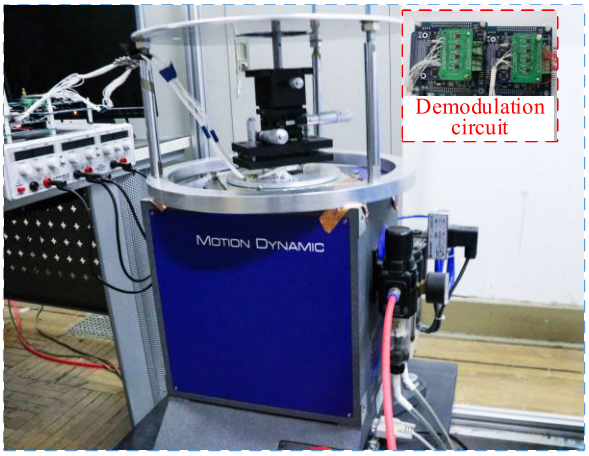

FIGURE 8. Experimental setup, which included a high-precision air-floating turntable (positional accuracy better than ±0.8 arcsec), a demodulation circuit, a computer for data acquisition, and a computer for turntable controlling.

TABLE 1. Initialization parameters of the IPSO algorithm.

Initial parameters	Value
Number of particles	50
Population size	20
Number of evolutions	20
Inertia factor ω	0.5
Learning factor c_1	1.6
Learning factor c_2	1.2

TABLE 2. Optimal parameters by IPSO of SVM.

Channel	C * 10^4	g * 10^4
First(N=119)	17.7904	188.1759
Second(N=120)	44.92858	264.8011
Third(N=179)	41.7114	826.7396
Fourth(N=180)	90.4874	395.8999

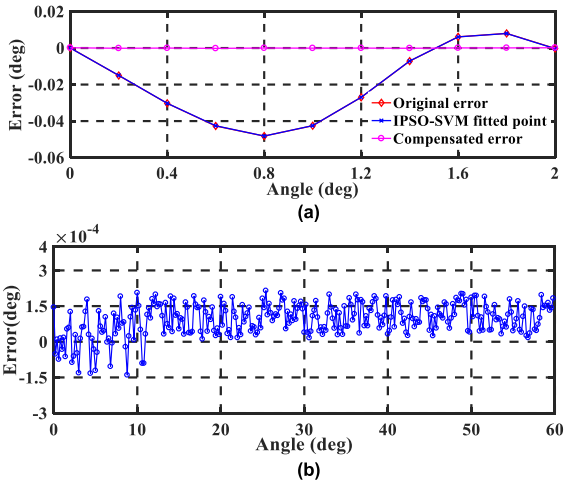

FIGURE 9. Compensated result with the number of petal-shape on 180. (a) Original and fitted point by IPSO-SVM; (b) compensated error from 0 to 60.

To further evaluate the IPSO-SVM method, the mean absolute error (MAE), average relative error (ARE) and root mean square error (RMSE) are applied as indices to evaluate

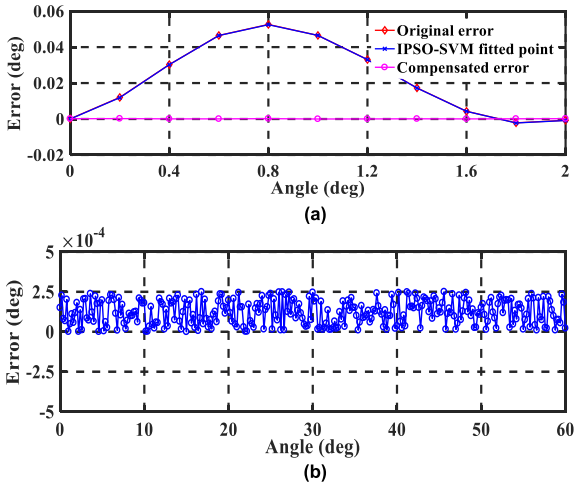

FIGURE 10. Compensated result with the number of petal-shape on 179. (a) Original and fitted point by IPSO-SVM; (b) compensated error from 0 to 60.

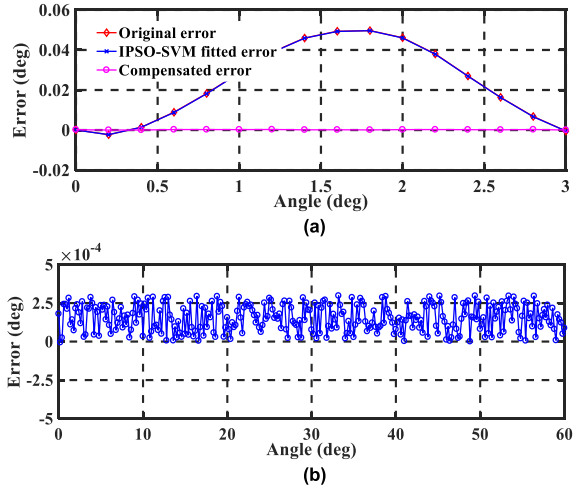

FIGURE 11. Compensated result with the number of petal-shape on 120. (a) Original and fitted point by IPSO-SVM; (b) compensated error from 0 to 60.

model performance. Their definitions are as follows:

$$MAE = \frac{1}{n} \cdot \sum_{i=1}^{n} \left| Y(i) - Y(i)^* \right| \tag{19}$$

$$ARE = \frac{1}{n} \cdot \sum_{i=1}^{n} \frac{|Y(i) - Y(i)^*|}{Y(i)} \tag{20}$$

$$RMSE = \sqrt{\frac{1}{n} \cdot \sum_{i=1}^{n} (Y(i) - Y(i)^*)^2} \tag{21}$$

where $Y(i)^*$ is the modeling value, $Y(i)$ is the actual value obtained via high-precision turntable, and n is number of testing samples.

The results of compensation via the LSM, BP-ANN, and IPSO-SVM methods are listed in Table 3 and shown in Figure 13. The dataset of 1, 2, 3, and 4 shown the compensation results of the encoders with 119, 120, 179, and 180 segments, respectively. It can be seen in the

TABLE 3. Performance comparison of three methods.

Method	MAE (*10^{-3})				ARE (*10^{-3})				RMSE (*10^{-3})			
Dataset	1	2	3	4	1	2	3	4	1	2	3	4
LSM	3.446	1.191	1.163	1.224	6.288	16.42	69.7	17.92	4.345	1.465	1.422	1.527
RBF-ANN	3.048	0.419	0.598	0.5615	-17.2	10.87	44.2	10.75	4.074	0.54	0.726	0.7031
IPSO-SVM	0.1469	0.1514	0.1226	0.1278	-0.728	0.5838	6.32	0.865	0.171	0.1751	0.1428	0.1468

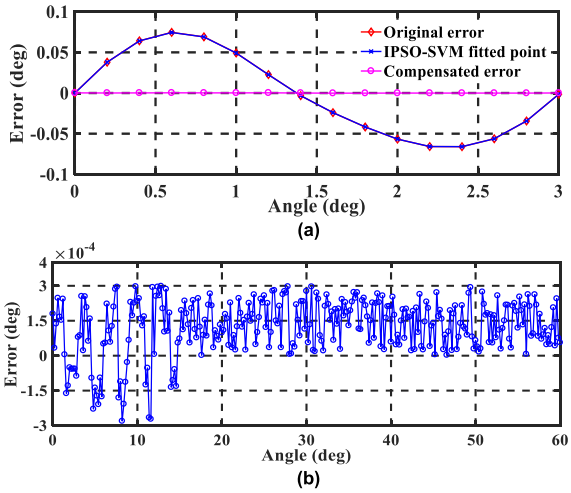

FIGURE 12. Compensated result with the number of petal-shape on 119. (a) Original and fitted point by IPSO-SVM; (b) compensated error from 0 to 60.

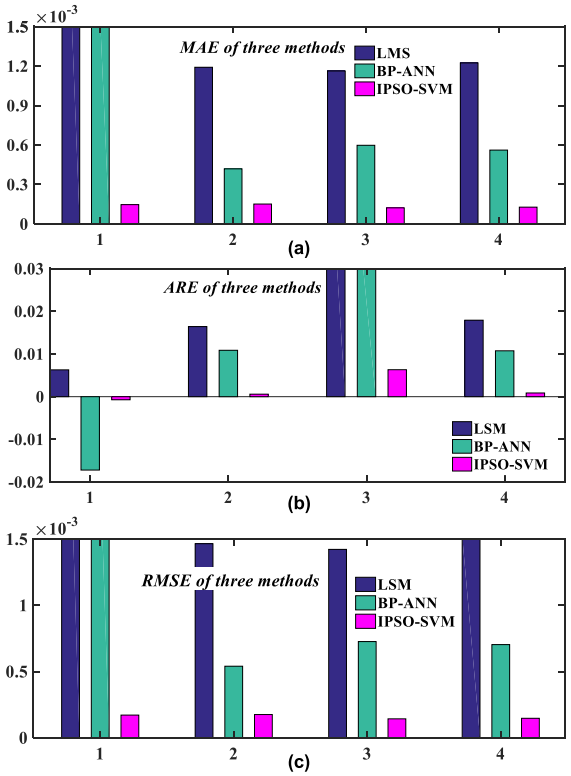

FIGURE 13. Results of the MAE, ARE, and RMSE evaluation of the LSM (a), BP-ANN (b), and IPSO-SVM (c) methods on the data from encoder: 1, 2, 3, and 4 shown the compensation results of the encoders with 119, 120, 179, and 180 segments, respectively.

figures that the IPSO-SVM algorithm demonstrated outstanding performance on three evaluation indicators compared to the LSM and ANN. The better compensation performance may be due to the global search capability of the IPSO algorithm and the effective regression classification of the SVM. IPSO-SVM combines both the advantages of PSO and SVM. The measurement accuracy of the four groups is shown in Table 4, where the accuracy after compensation via the IPSO-SVM algorithm was below 0.0005°.

TABLE 4. The nonlinear error before and after compensation adopts the IPSOSVM method.

Group	$N = 119$	$N = 120$	$N = 179$	$N = 180$
Before compensation (°)	0.17	0.16	0.08	0.08
After compensation (°)	0.0006	0.00052	0.0005	0.00045

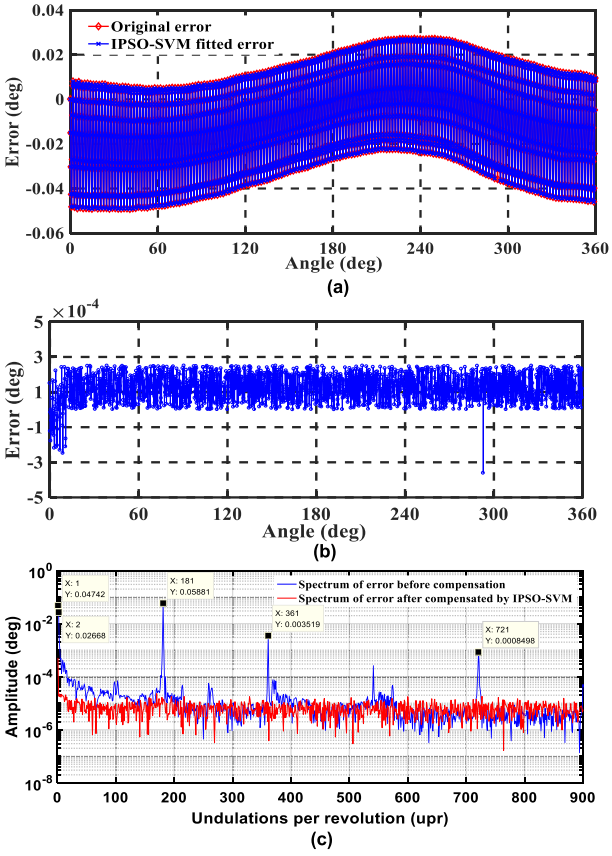

FIGURE 14. Nonlinearity error after compensation by IPSO-SVM method of an encoder with 180 subdivide numbers. (a) Error compensation over the full measurement range. (b) Compensated nonlinear error from 0° to 360°. (c) Error spectrum before and after compensation.

The results after the compensation is shown in Fig. 14(a), (b), and (c). The nonlinear error of the sensor is reduced to less than 0.0002° over the full range, which indicates the capacitive encoder has great potential to be applied in high-precision applications with low cost.

Figure 14(a) and (b) show the error distribution over the full-scale range of a capacitive angular displacement sensor with 180 segments after compensation via the IPSO-SVM algorithm. In the figure, it can be seen the nonlinear errors were effectively reduced and the error after compensation over the full-scale measurement range from 0° to 360° did not exceed 0.0005°. The periodic nonlinear was almost totally eliminated. A spectral analysis before and after compensation is shown Figure 14(c), where it can be seen that the compensation was sufficient to overcome the periodic nonlinear errors. These results indicate the algorithm significantly improved the measurement accuracy of the capacitive angular encoder.

VII. CONCLUSION

The focus of this research was to develop a method to compensate the periodic nonlinear which effected by installation, processing, and demodulation circuit errors. The proposed nonlinear error compensation method is based on an improved particle swarm optimization (IPSO) method and support vector machine (SVM). The IPSO algorithm was adopted to determine optimal parameters of the SVM algorithm to further improve the precision of the compensation results. The proposed method was validated, the results showed that the compensation provided by the IPSO-SVM method was able to reduce the nonlinear error from 0.08° to 0.0005° which is better than LSM and ANN. This method can be widely used in the error compensation and effectively improve the measurement accuracy of the encoder. In the future, more efficient and simple compensation algorithms should be studied.

REFERENCES

[1] M. Gasulla, X. Li, G. C. M. Meijer, L. van der Ham, and J. W. Spronck, "A contactless capacitive angular-position sensor," *IEEE Sensors J.*, vol. 3, no. 5, pp. 607–614, Oct. 2003.

[2] L. Ben-Brahim, M. Benammar, and M. A. Alhamadi, "A resolver angle estimator based on its excitation signal," *IEEE Trans. Ind. Electron.*, vol. 56, no. 2, pp. 574–580, Feb. 2009.

[3] K. Peng, Z. Yu, X. Liu, Z. Chen, and H. Pu, "Features of capacitive displacement sensing that provide high-accuracy measurements with reduced manufacturing precision," *IEEE Trans. Ind. Electron.*, vol. 64, no. 9, pp. 7377–7386, Sep. 2017.

[4] D. Zheng, S. Zhang, S. Wang, C. Hu, and X. Zhao, "A capacitive rotary encoder based on quadrature modulation and demodulation," *IEEE Trans. Instrum. Meas.*, vol. 64, no. 1, pp. 143–153, Jan. 2015.

[5] D. Krklješ, D. Vasiljević, and G. Stojanović, "A capacitive angular sensor with flexible digitated electrodes," *Sensor Rev.*, vol. 34, no. 4, pp. 382–388, Aug. 2014.

[6] B. Hou, B. Zhou, M. Song, Z. Lin, and R. Zhang, "A novel single-excitation capacitive angular position sensor design," *Sensors*, vol. 16, no. 8, p. 1196, Jul. 2016.

[7] Z. Zhang, F. Ni, Y. Dong, C. Guo, M. Jin, and H. Liu, "A novel absolute magnetic rotary sensor," *IEEE Trans. Ind. Electron.*, vol. 62, no. 7, pp. 4408–4419, Jul. 2015.

[8] B. Hou, Z. Tian, C. Li, Q. Wei, B. Zhou, and R. Zhang, "A capacitive rotary encoder with a novel sensitive electrode," in *Proc. IEEE Sensors*, Glasgow, U.K., Oct./Nov. 2017, pp. 1–3.

[9] M. Karali, A. T. Karasahin, O. Keles, M. Kocak, and M. A. Erismis, "A new capacitive rotary encoder based on analog synchronous demodulation," *Electr. Eng.*, vol. 100, no. 3, pp. 1975–1983, Sep. 2018.

[10] B. Hou, B. Zhou, X. Li, B. Xing, L. Yi, Q. Wei, and R. Zhang, "Periodic nonlinear error analysis and compensation of a single-excited petal-shaped capacitive encoder to achieve high-accuracy measurement," *Sensors*, vol. 19, no. 10, p. 2412, May 2019.

[11] S.-H. Hwang, H.-J. Kim, J.-M. Kim, L. Liu, and H. Li, "Compensation of amplitude imbalance and imperfect quadrature in resolver signals for PMSM drives," *IEEE Trans. Ind. Appl.*, vol. 47, no. 1, pp. 134–143, Jan. 2011.

[12] C. Cecati, J. Kolbusz, P. Rozycki, P. Siano, and B. M. Wilamowski, "A novel RBF training algorithm for short-term electric load forecasting and comparative studies," *IEEE Trans. Ind. Electron.*, vol. 62, no. 10, pp. 6519–6529, Oct. 2015.

[13] S. Chong, S. Rui, L. Jie, Z. Xiaoming, T. Jun, S. Yunbo, L. Jun, and C. Huiliang, "Temperature drift modeling of MEMS gyroscope based on genetic-Elman neural network," *Mech. Syst. Signal Process.*, vols. 72–73, pp. 897–905, May 2016.

[14] X. Z. Li and J. M. Kong, "Application of GA-SVM method with parameter optimization for landslide development prediction," *Natural Hazards Earth Syst. Sci.*, vol. 14, no. 3, pp. 525–533, Mar. 2014.

[15] X. Meng, P. Rozycki, J.-F. Qiao, and B. M. Wilamowski, "Nonlinear system modeling using RBF networks for industrial application," *IEEE Trans. Ind. Informat.*, vol. 14, no. 3, pp. 931–940, Mar. 2018.

[16] H. Pang, J. Li, D. Chen, M. Pan, S. Luo, Q. Zhang, and F. Luo, "Calibration of three-axis fluxgate magnetometers with nonlinear least square method," *Measurement*, vol. 46, no. 4, pp. 1600–1606, May 2013.

[17] S. A. Khan, D. T. Shahani, and A. K. Agarwala, "Sensor calibration and compensation using artificial neural network," *ISA Trans.*, vol. 42, no. 3, pp. 337–352, Jul. 2003.

[18] J. Li, G. Hu, Y. Zhou, C. Zou, W. Peng, and J. Alam SM, "Study on temperature and synthetic compensation of piezo-resistive differential pressure sensors by coupled simulated annealing and simplex optimized kernel extreme learning machine," *Sensors*, vol. 17, no. 4, p. 894, Apr. 2017.

[19] Y. Sun, Y. Liu, and H. Liu, "Temperature compensation for a six-axis force/torque sensor based on the particle swarm optimization least square support vector machine for space manipulator," *IEEE Sensors J.*, vol. 16, no. 3, pp. 798–805, Feb. 2016.

[20] S. Liu, L. Xu, Q. Li, X. Zhao, and D. Li, "Fault diagnosis of water quality monitoring devices based on multiclass support vector machines and rule-based decision trees," *IEEE Access*, vol. 6, pp. 22184–22195, 2018.

[21] H. Xing, B. Hou, Z. Lin, and M. Guo, "Modeling and compensation of random drift of MEMS gyroscopes based on least squares support vector machine optimized by chaotic particle swarm optimization," *Sensors*, vol. 17, no. 10, p. 2335, Oct. 2017.

[22] M. Jiang, L. Jiang, D. Jiang, J. Xiong, J. Shen, S. H. Ahmed, J. Luo, and H. Song, "Dynamic measurement errors prediction for sensors based on firefly algorithm optimize support vector machine," *Sustain. Cities Soc.*, vol. 35, pp. 250–256, Nov. 2017.

[23] M. Jiang, J. Luo, D. Jiang, J. Xiong, H. Song, and J. Shen, "A cuckoo search-support vector machine model for predicting dynamic measurement errors of sensors," *IEEE Access*, vol. 4, pp. 5030–5037, 2016.

[24] Y. Chuan and L. Chen, "The application of support vector machine in the hysteresis modeling of silicon pressure sensor," *IEEE Sensors J.*, vol. 11, no. 9, pp. 2022–2026, Sep. 2011.

[25] Z. Zhong, S. Liu, M. Kazemi, and T. R. Carr, "Dew point pressure prediction based on mixed-kernels-function support vector machine in gas-condensate reservoir," *Fuel*, vol. 232, pp. 600–609, Nov. 2018.

[26] X. Mao, Y. Wang, X. Liu, and Y. Guo, "A hybrid feedforward-feedback hysteresis compensator in piezoelectric actuators based on least-squares support vector machine," *IEEE Trans. Ind. Electron.*, vol. 65, no. 7, pp. 5704–5711, Jul. 2018.

[27] P. Lu, L. Ye, B. Sun, C. Zhang, Y. Zhao, and J. Teng, "A new hybrid prediction method of ultra-short-term wind power forecasting based on EEMD-PE and LSSVM optimized by the GSA," *Energies*, vol. 11, no. 4, p. 697, Mar. 2018.

[28] M. Jiang, L. Jiang, D. Jiang, F. Li, and H. Song, "A sensor dynamic measurement error prediction model based on NAPSO-SVM," *Sensors*, vol. 18, no. 2, p. 233, Jan. 2018.

[29] P. Chen, Y. Xie, P. Jin, and D. Zhang, "A wireless sensor data-based coal mine gas monitoring algorithm with least squares support vector machines optimized by swarm intelligence techniques," *Int. J. Distrib. Sensor Netw.*, vol. 14, no. 5, May 2018, Art. no. 155014771877744.

[30] M. Karimi, "A new approach to history matching based on feature selection and optimized least square support vector machine," *J. Geophys. Eng.*, vol. 15, no. 6, pp. 2378–2387, Dec. 2018.

[31] J. Cheng, J. Fang, W. Wu, and J. Li, "Temperature drift modeling and compensation of RLG based on PSO tuning SVM," *Measurement*, vol. 55, pp. 246–254, Sep. 2014.

[32] G. Wei, G. Li, Y. Wu, and X. Long, "Application of least squares-support vector machine in system-level temperature compensation of ring laser gyroscope," *Measurement*, vol. 44, no. 10, pp. 1898–1903, Dec. 2011.

BO HOU (Graduate Student Member, IEEE) was born in Sichuan, China, in 1991. He received the B.Sc. degree from Chongqing University, in 2015. He is currently pursuing the Ph.D. degree with the State Key Laboratory of Precision Measuring Technology and Instruments, Tsinghua University, Beijing, China. His main research interests include MEME inertia sensor and angular sensor.

BIN ZHOU received the B.S. and Ph.D. degrees in precision instruments from Tsinghua University, Beijing, China, in 1998 and 2004, respectively. From 2004 to 2010, he was an Assistant Professor of MEMS inertial sensor with the Department of Precision Instruments, Tsinghua University. Since 2010, he has been an Associate Professor with Tsinghua University. His interests are in the fields of MEMS inertial sensors, digital signal process, and sensor ASIC design.

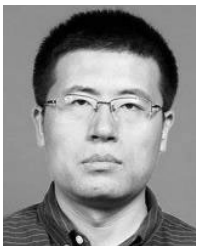

XIANG LI received the bachelor's degree from Tsinghua University, Beijing, China, in 2011, where he is currently pursuing the master's degree. His research interests are in the area of MEMS gyroscopes, inertial navigation systems, and analog integrated circuit design.

LUYING YI was born in Inner Mongolia, China, in 1994. She received the B.S. degree in information engineering from Tianjin University, in 2015. She is currently pursuing the Ph.D. degree in optical engineering with the Department of Precision Instruments, Tsinghua University, Beijing, China. Her research interests include spectrum measurement technology, optical sensing, and bio-optics.

QI WEI received the Ph.D. degree from Tsinghua University, Beijing, China, in 2010. He is currently an Associate Professor with the Department of Precision Instruments, Tsinghua University. His research interests are MEMS inertial sensors ASIC design and high performance data converters.

RONG ZHANG received the B.S. degree in mechanical design and manufacturing and the M.S. and Ph.D. degrees in precision instruments from Tsinghua University, Beijing, China, in 1992 and 2007, respectively. He joined the Faculty Member of Tsinghua University, in 1994. He became a Professor at the Department of Precision Instrument, Tsinghua University. His professional interests include the precision motion control system, MEMS inertial sensors, and integrated navigation systems.